In vivo optical frequency domain imaging of human retina and choroid

Edward C. W. Lee[1, 2], Johannes F. de Boer[1], Mircea Mujat[1], Hyungsik Lim[1] and Seok H. Yun[1]

[1]*Harvard Medical School and Wellman Center for Photomedicine, Massachusetts General Hospital 50 Blossom Street, Boston, Massachusetts 02114*
[2]*Department of Electrical Engineering and Computer Science, Massachusetts Institute of Technology 77 Massachusetts Avenue, Cambridge, Massachusetts 02139*
syun@hms.harvard.edu

Abstract: Optical frequency domain imaging (OFDI) using swept laser sources is an emerging second-generation method for optical coherence tomography (OCT). Despite the widespread use of conventional OCT for retinal disease diagnostics, until now imaging the posterior eye segment with OFDI has not been possible. Here we report the development of a high-performance swept laser at 1050 nm and an ophthalmic OFDI system that offers an A-line rate of 18.8 kHz, sensitivity of >92 dB over a depth range of 2.4 mm with an optical exposure level of 550 μW, and deep penetration into the choroid. Using these new technologies, we demonstrate comprehensive human retina, optic disc, and choroid imaging *in vivo*. This advance enables us to view choroidal vasculature *in vivo* without intravenous injection of fluorescent dyes and may provide a useful tool for evaluating choroidal as well as retinal diseases.

OCIS codes: (110.4500) Optical coherence tomography; (120.3180) Interferometry; (140.3600) Lasers, tunable; (170.3880) Medical and biological imaging; (170.4470) Ophthalmology; (330.4460) Ophthalmic optics

References and links

1. A. F. Fercher, W. Drexler, C. K. Hitzenberger, and T. Lasser, "Optical coherence tomography - principles and applications," Rep. Prog. Phys. **66**, 239-303 (2003).
2. S. R. Chinn, E. A. Swanson, and J. G. Fujimoto, "Optical coherence tomography using a frequency-tunable optical source," Opt. Lett. **22**, 340-342 (1997).
3. S. H. Yun, G. J. Tearney, J. F. de Boer, N. Iftimia, and B. E. Bouma, "High-speed optical frequency-domain imaging," Opt. Express **11**, 2953-2963 (2003),.
4. M. A. Choma, M. V. Sarunic, C. H. Yang, and J. A. Izatt, "Sensitivity advantage of swept source and Fourier domain optical coherence tomography," Opt. Express **11**, 2183-2189 (2003),.
5. H. Barfuss, and E. Brinkmeyer, "Modified optical frequency-domain reflectometry with high spatial-resolution for components of integrated optic systems," J. Lightwave Technol. **7**, 3-10 (1989).
6. S. H. Yun, G. J. Tearney, J. F. de Boer, M. Shishkov, W. Y. Oh, and B. E. Bouma, "Catheter-based optical frequency domain imaging at 36 frames per second," in *Coherence Domain Optical Methods and Optical Coherence Tomography in Biomedicine IX, 5690-16*(San Jose, CA, 2005).
7. B. J. Vakoc, S. H. Yun, M. S. Shishkov, W. Oh, J. A. Evans, N. S. Nishioka, B. E. Bouma, and G. J. Tearney, "Comprehensive microscopy of the esophagus using optical frequency domain imaging," in *Coherence Domain Optical Methods and Optical Coherence Tomography in Biomedicine X, 6082-13*(San Jose, CA, 2006).
8. R. Huber, M. Wojtkowski, J. G. Fujimoto, J. Y. Jiang, and A. E. Cable, "Three-dimensional and C-mode OCT imaging with a compact, frequency swept laser source at 1300 nm," Opt. Express **13**, 10523-10538 (2005).
9. Y. Yasuno, V. D. Madjarova, S. Makita, M. Akiba, A. Morosawa, C. Chong, T. Sakai, K. P. Chan, M. Itoh, and T. Yatagai, "Three-dimensional and high-speed swept-source optical coherence tomography for in vivo investigation of human anterior eye segments," Opt. Express **13**, 10652-10664 (2005).
10. J. Zhang, and Z. P. Chen, "In vivo blood flow imaging by a swept laser source based Fourier domain optical Doppler tomography," Opt. Express **13**, 7449-7457 (2005).

#68653 - $15.00 USD Received 7 March 2006; revised 25 April 2006; accepted 27 April 2006

11. M. A. Choma, K. Hsu, and J. A. Izatt, "Swept source optical coherence tomography using an all-fiber 1300-nm ring laser source," J Biomed Opt **10**, 44009 (2005).
12. R. Huber, M. Wojtkowski, K. Taira, J. G. Fujimoto, and K. Hsu, "Amplified, frequency swept lasers for frequency domain reflectometry and OCT imaging: design and scaling principles," Opt. Express **13**, 3513-3528 (2005).
13. M. R. Hee, J. A. Izatt, E. A. Swanson, D. Huang, J. S. Schuman, C. P. Lin, C. A. Puliafito, and J. G. Fujimoto, "Optical Coherence Tomography of the Human Retina," Arch. Opthalmol. **113**, 325-332 (1995).
14. C. A. Puliafito, M. R. Hee, C. P. Lin, E. Reichel, J. S. Schuman, J. S. Duker, J. A. Izatt, E. A. Swanson, and J. G. Fujimoto, "Imaging of Macular Diseases with Optical Coherence Tomography," Ophthalmology **102**, 217-229 (1995).
15. A. Unterhuber, B. Povazay, B. Hermann, H. Sattmann, A. Chavez-Pirson, and W. Drexler, "In vivo retinal optical coherence tomography at 1040 nm-enhanced penetration into the choroid," Opt. Express **13**, 3252-3258 (2005).
16. S. Bourquin, A. D. Aguirre, I. Hartl, P. Hsiung, T. H. Ko, J. G. Fujimoto, T. A. Birks, W. J. Wadsworth, U. Bunting, and D. Kopf, "Ultrahigh resolution real time OCT imaging using a compact femtosecond Nd : Glass laser and nonlinear fiber," Opt. Express **11**, 3290-3297 (2003).
17. H. Lim, Y. Jiang, Y. M. Wang, Y. C. Huang, Z. P. Chen, and F. W. Wise, "Ultrahigh-resolution optical coherence tomography with a fiber laser source at 1 μm," Opt. Lett. **30**, 1171-1173 (2005).
18. M. Wojtkowski, R. Leitgeb, A. Kowalczyk, T. Bajraszewski, and A. F. Fercher, "In vivo human retinal imaging by Fourier domain optical coherence tomography," J. Biomed. Opt. **7**, 457-463 (2002).
19. N. A. Nassif, B. Cense, B. H. Park, M. C. Pierce, S. H. Yun, B. E. Bouma, G. J. Tearney, T. C. Chen, and J. F. de Boer, "In vivo high-resolution video-rate spectral-domain optical coherence tomography of the human retina and optic nerve," Opt. Express **12**, 367-376 (2004).
20. S. H. Yun, G. J. Tearney, J. F. de Boer, and B. E. Bouma, "Motion artifacts in optical coherence tomography with frequency-domain ranging," Opt. Express **12**, 2977-2998 (2004).
21. M. V. Shramenko, E. V. Andreeva, D. S. Mamedov, V. R. Shidlovski, and S. D. Yakubovich, "NIR semiconductor laser with fast broadband tuning," in *Coherence Domain Optical Methods and Optical Coherence Tomography in Biomedicine X, 6079-42*(2006).
22. F. D. Nielsen, L. Thrane, J. Black, K. Hsu, A. Bjarklev, and P. E. Andersen, "Swept-Wavelength Source for Optical Coherence Tomography in the 1 μm Range," in *European Congress on Biomedical Optics (ECBO)*(Munich, Germany, 12-16 June 2005).
23. S. H. Yun, C. Boudoux, G. J. Tearney, and B. E. Bouma, "High-speed wavelength-swept semiconductor laser with a polygon-scanner-based wavelength filter," Opt. Lett. **28**, 1981-1983 (2003).
24. B. Cense, H. C. Chen, B. H. Park, M. C. Pierce, and J. F. de Boer, "In vivo birefringence and thickness measurements of the human retinal nerve fiber layer using polarization-sensitive optical coherence tomography," J. Biomed. Opt. **9**, 121-125 (2004).
25. American National Standards Institute, *American national standard for safe use of lasers z136.1* (American National Standards Institute, Orlando, FL, 2000).
26. D. J. Segelstein, *The complex refractive index of water* (University of Missouri-Kansas City, 1981).
27. B. Cense, N. A. Nassif, T. C. Chen, M. C. Pierce, S. H. Yun, B. H. Park, B. E. Bouma, G. J. Tearney, and J. F. de Boer, "Ultrahigh-resolution high-speed retinal imaging using spectral-domain optical coherence tomography," Opt. Express **12**, 2435-2447 (2004).
28. S. L. Jiao, R. Knighton, X. R. Huang, G. Gregori, and C. A. Puliafito, "Simultaneous acquisition of sectional and fundus ophthalmic images with spectral-domain optical coherence tomography," Opt. Express **13**, 444-452 (2005).
29. M. Mujat, R. C. Chan, B. Cense, B. H. Park, C. Joo, T. Akkin, T. C. Chen, and J. F. de Boer, "Retinal nerve fiber layer thickness map determined from optical coherence tomography images," Opt. Express **13**, 9480-9491 (2005).
30. V. Poukens, B. J. Glasgow, and J. L. Demer, "Nonvascular contractile cells in sclera and choroid of humans and monkeys," Invest. Ophthalmol. Visual Sci. **39**, 1765-1774 (1998).
31. D. V. Alfaro, P. E. Liggett, W. F. Mieler, H. Quiroz-Mercado, R. D. Jager, and Y. Tano, *Age-related macular degneration: a comprehensive textbook* (Lippincott Williams & Wilkins, Philadelphia, PA, 2006).
32. F. C. Delori, E. S. Gragoudas, R. Francisco, and R. C. Pruett, "Monochromatic Ophthalmoscopy and Fundus Photography - Normal Fundus," Arch. Opthalmol. **95**, 861-868 (1977).
33. R. H. Webb, G. W. Hughes, and F. C. Delori, "Confocal Scanning Laser Ophthalmoscope," Appl. Opt. **26**, 1492-1499 (1987).
34. F. G. Holz, C. Bellmann, K. Rohrschneider, R. O. W. Burk, and H. E. Volcker, "Simultaneous confocal scanning laser fluorescein and indocyanine green angiography," Am. J. Opthalmol. **125**, 227-236 (1998).

1. Introduction

Optical frequency domain imaging (OFDI), also known as swept source optical coherence tomography (OCT), is a new method for OCT that uses a wavelength-swept light source to probe the amplitude and phase of back scattering light from tissue [1-3]. This frequency-

#68653 - $15.00 USD Received 7 March 2006; revised 25 April 2006; accepted 27 April 2006

domain method offers intrinsic signal-to-noise ratio (SNR) advantage over the time-domain method [4, 5]. With the recently developed rapidly tunable lasers in the 1300-nm range, OFDI has enabled significant improvements in imaging speed, sensitivity, and ranging depth over conventional time-domain OCT systems and been demonstrated for imaging skin, coronary artery, esophagus, and anterior eye segments [3, 6-12]. While retinal imaging is the most established clinical use of OCT, this application has been out of reach for the OFDI systems developed to date because the optical absorption in human eye at 1300 nm is too large. The standard spectral range of conventional ophthalmic OCT has been between 700 and 900 nm where the humors in the eye are transparent and broadband super-luminescent-diode (SLD) light sources are readily available [13, 14]. Recent studies have suggested that the 1040-nm spectral range [15-17] could be a viable alternative operating window for retinal imaging and potentially could offer deeper penetration into the choroid below the highly absorbing and scattering retinal pigment epithelium [15]. Spectral domain (SD) OCT, also known as Fourier domain OCT, using broadband light sources at 800 nm and spectrometers has been developed to enable three-dimensional retinal imaging *in vivo* with superior image acquisition speed and sensitivity to conventional time-domain OCT [18, 19]. Compared to SD-OCT, OFDI offers several advantages, such as immunity to motion-induced signal fading [20], simple polarization-sensitive or diversity scheme [6], and long ranging depth [3]. Until now, however, a clinical-viable OFDI system for imaging posterior eye segments has been unavailable, primarily due to the lack of a wide-tuning rapidly-swept light source in the low water absorption window [2, 21, 22].

In this paper, we report the development of a high-performance wavelength-swept laser with a center wavelength at 1050 nm. Using an OFDI system employing the laser source, we demonstrate the first OFDI imaging of posterior segments of the human eye *in vivo* with high image acquisition speed, sensitivity, and penetration depth.

2. Experimental setup

2.1 Laser

Figure 1(a) depicts a schematic of the laser source we developed in a linear-cavity configuration. The gain medium was a commercially-available, bi-directional semiconductor optical amplifier (QPhotonics, Inc., QSOA-1050) driven at an injection current level of 400 mA. One port of the amplifier was coupled to a wavelength-scanning filter [23] that comprised a diffraction grating (1200 lines/mm), a telescope (f_1 = 100 mm, f_2 = 50 mm), and a polygon mirror scanner (Lincoln Lasers, Inc., 40 facets). The design bandwidth and free spectral range of the filter were ~0.1 nm and 61 nm, respectively. The amplifier's other port was spliced to a loop mirror made of a 50/50 coupler. The Sagnac loop also served as an output coupler. The reflectivity and output coupling ratio were complementary and optimized by adjusting a polarization controller (PC_1) to tune the amount of birefringence-induced non-reciprocity in the loop. The linear-cavity configuration is an attractive alternative to the previous ring-cavity design [23] as low-loss, low-cost circulators and isolators are not readily available at 1050 nm. Sweep repetition rates of up to 36 kHz were possible with 100% duty cycle, representing a significant improvement over previously demonstrated swept lasers that offered tuning rates of a few hundred Hz in the 1050-nm range and below [2, 21, 22]. Due to the limited sampling speed of the data acquisition board in our OFDI system described next, we operated the laser at a wavelength sweep rate of 18.8 kHz to obtain a sufficient depth range. The laser output was singly polarized with an average power of 2.7 mW.

#68653 - $15.00 USD Received 7 March 2006; revised 25 April 2006; accepted 27 April 2006

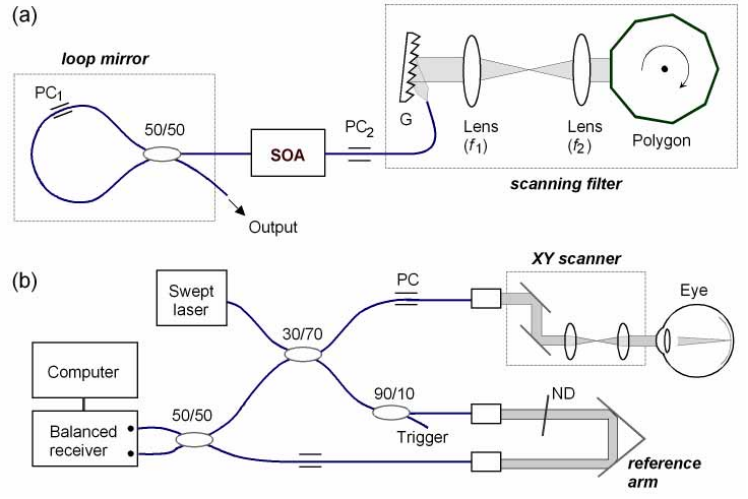

Fig. 1. Experimental setup: (a) wavelength-swept laser and (b) OFDI system.

2.2 Imaging system

Using the swept laser as a light source, we constructed an OFDI system (Fig. 1(b)). The system further comprised a fiber-optic interferometer, a beam scanner, detection electronics and a computer. The sample arm (30% port) was connected to a human interface designed for retinal imaging [24]. The focal beam size was approximately 10 μm in tissue (index = 1.38). The optical power level at the entrance pupil of the eye was measured to be 550 μW, well below the 1.9-mW maximum exposure level at λ=1050 nm according to the ANSI laser safety standard for continuous exposure [25]. The reference arm (70% port) employed a transmission-type variable delay line and a 10% tap coupler to generate sampling trigger signals for data acquisition [3]. A neutral-density (ND) attenuator was used to obtain the optimal reference-arm power. Light returning from the sample was combined with the reference light at a 50/50 coupler. Resulting interference signals were measured with an InGaAs dual-balanced detector (New Focus, Inc., 1811). The detector signal was further amplified (10 dB), low-pass filtered (DC to 5 MHz), and digitized at 10 MS/s with a 12-bit data acquisition board (National Instruments, Inc., PCI-6115) [3]. A total of 512 samples were acquired during each A-line scan. The imaging depth range determined by the spectral sampling interval was 2.44 mm in air.

3. Results

3.1 Laser output characteristics

Figure 2(a) depicts the output spectrum measured with an optical spectrum analyzer in peak-hold mode (resolution = 0.1 nm). The output spectrum spanned from 1019 to 1081 nm over a range of 62 nm determined by the free spectral range of the filter. The spectral range coincided with a local transparent window of the eye. The roundtrip optical absorption in human vitreous and aqueous humors is estimated to be 3 - 4 dB based on known absorption characteristics of water (Fig. 2(a)) [26]. Using a variable-delay Michelson interferometer, we measured the coherence length of the laser output, defined as the roundtrip delay resulting in 50% reduction in interference fringe visibility, to be approximately 4.4 mm in air. From this value, we calculated the instantaneous linewidth of laser output to be 0.11 nm. Figure 2(b) depicts an oscilloscope trace of laser output showing 100% tuning duty cycle at 18.8 kHz (single shot, 5-MHz detection bandwidth). The y-axis of the trace represents instantaneous

#68653 - $15.00 USD Received 7 March 2006; revised 25 April 2006; accepted 27 April 2006

optical power. When lasing was suppressed by blocking the intracavity beam in the polygon filter, the total power of amplified spontaneous emission (ASE) in the output was 0.5 mW. Since ASE is significantly suppressed during lasing, we expect that the ASE level in the laser output should be much lower. The laser output exhibited significant intensity fluctuations (~8%pp) due to an etalon effect originating from relatively large facet reflections at the SOA chip with a thickness equivalent to 2.5 mm in air. In the imaging system, the delayed optical waves by etalon reflection can cause ghost images; however, due to their relatively low magnitudes, we did not observe the artifacts in retinal imaging.

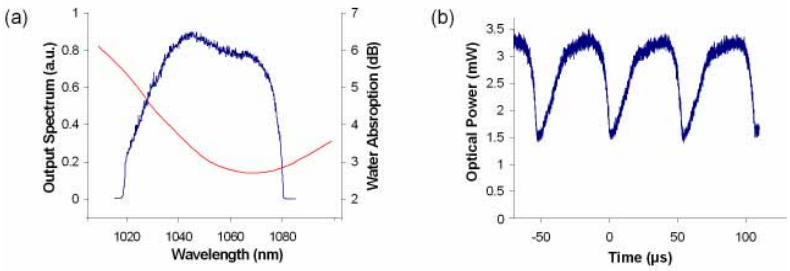

Fig. 2. Measured laser output characteristics. (a) Peak-hold output spectrum (blue curve) and optical absorption in water (red curve) for 42-mm propagation distance corresponding to a roundtrip in typical human vitreous. (b) Time-domain output trace.

3.2 System sensitivity and resolution

We characterized the OFDI system and optimized operating parameters to maximize the SNR using a partial reflector (ND attenuator and gold-coated mirror) as a sample. Optimal reference arm power for maximum SNR was determined to be 2.6 μW at each detection port. This relatively low value is attributed to the relatively large intensity noise of the laser that could not be completely suppressed in the dual balanced detection. Data processing took several steps, including background subtraction, envelope apodization (windowing), interpolation into linear k-space [3], and dispersion correction [27]. The background data was obtained by temporarily blocking the sample arm [3]. Subtracting this background from the interference signals eliminates fixed-pattern artifacts at low frequencies (depths). Apodizing the interference fringes by imposing a proper windowing method can decrease the sidebands of point spread functions and improve image contrast. This process, however, comes at the cost of resolution loss and SNR reduction, because the windowing reduces the effective integration time, or spectral range, in the Fourier transform. We used a Gaussian window to yield a desirable compromise in contrast and resolution. Since the detector signal was sampled in constant time intervals whereas the tuning curve of our laser was nonlinear in k-space, interpolating the interference signal was necessary to avoid image blurring. After the interpolation, the signal was further corrected for the chromatic dispersion in the interferometer as well as in the sample by multiplying with a proper phase function.

Figure 3 depicts the A-line profiles or point spread functions measured at various path length differences of the interferometer. For this measurement, we used a partial-reflector (-73 dB) in the sample arm, and the path length was varied by moving the reference mirror. The maximum SNR was 25 dB which corresponds to a maximum sensitivity of 98 dB. The theoretical shot-noise limit of sensitivity was calculated to be 109 dB; the 11-dB deficiency in sensitivity of our system seems reasonable, considering that the residual laser intensity noise, imperfect polarization alignment between the sample and reference light, and Gaussian windowing, among many other practical details, contributed to SNR loss. The non-flat frequency response of the low-pass filter, with variations of ~5 dB from DC to 5 MHz, was corrected for, resulting in a flat noise floor in Fig. 3. Sensitivity decreased to 92 dB as the

#68653 - $15.00 USD Received 7 March 2006; revised 25 April 2006; accepted 27 April 2006

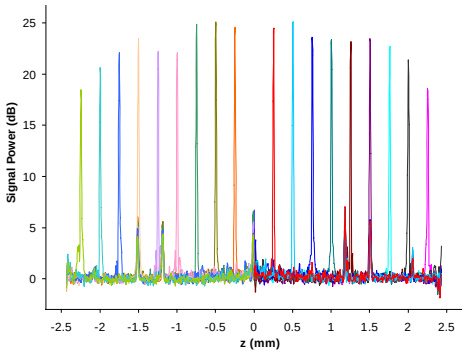

Fig. 3. Point spread functions measured at various path length differences for a sample reflectivity of -73 dB. To facilitate SNR analysis, each curve plotted was obtained by averaging over 500 consecutive scans at constant depth, and a simple numerical subtraction was performed to make the noise floor flat.

path length increased to a depth of 2.4 mm, due to the finite coherence length of the laser output. Compared to the previous time-domain system using a broadband source at 1040 nm (50-nm bandwidth and 10-μm resolution in air) [15], our system offers higher sensitivity at a 100-fold faster image acquisition speed and one sixth of sample arm power. The high sensitivity and depth range of our system compare favorably with those of state-of-the-art spectral domain systems using broadband sources in the 700 – 900 nm spectral range [18, 19, 27]. Due to absorption by water in the eye, the actual SNR for the human retina would be 3 - 4 dB lower than the values measured with the mirror sample. Based on the source spectrum (Fig. 2(a)) and the Gaussian window function used, the theoretical axial resolution was calculated to be 13 μm in air; the measured values were 14 - 16 μm, increasing with the depth. Errors in interpolation and dispersion compensation due to higher order terms probably account for the discrepancy.

3.3 Video-rate imaging of retina, optic disc, and choroid in vivo

OFDI imaging was conducted with two healthy volunteers (A: 36-year-old Asian male, B: 41-year-old Caucasian male). The OFDI system acquired 20,000 A-lines continuously over 10.6 seconds as the focused sample beam was scanned over an area of 6 mm (horizontal) by 5.2 mm (vertical) across the macular region in the retina. Figure 4 depicts a movie sequence of the images recorded from volunteer A at a frame rate of 18.8 Hz. Each image frame was constructed from a thousand A-line scans with an inverse grayscale table mapping to the reflectivity range (47 dB). The anatomical layers in the retina are clearly visualized and

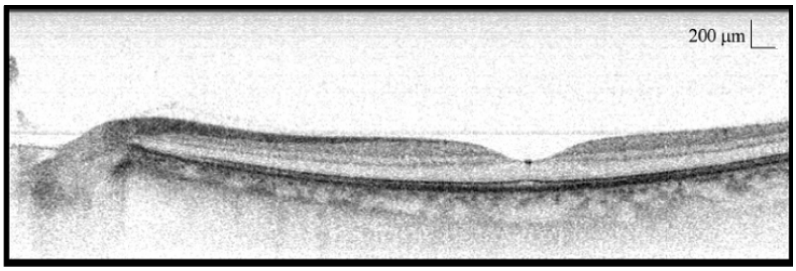

Fig. 4. (2.4 MB) A sequence of OFDI retina and choroid images obtained from a healthy volunteer. Each image frame consists of 1000 axial lines and spans over 6.0 mm (horizontal) and 1.8 mm (depth) in tissue. A total of 200 frames were acquired over 10.6 seconds to screen a tissue area with a vertical span of 5.2 mm. Only 120 frames are shown in the movie. The image above shows the fovea and optic disc. (11 MB version)

#68653 - $15.00 USD Received 7 March 2006; revised 25 April 2006; accepted 27 April 2006

correlate well with previously published OCT images and histological findings. Figure 5(A) depicts an expanded image of fovea extracted from the three-dimensional data set. The OFDI image provides deep penetration into the choroid nearly up to the interface with the sclera, visualizing densely-packed choroidal capillaries and vessels.

To assess the penetration of our system, we performed three-dimensional imaging on the two volunteers A and B with both the OFDI system and a state-of-the-art SD-OCT system previously developed for video-rate retinal imaging [19]. The SD-OCT system employed a super luminescent diode with a center wavelength of 840 nm and a 3-dB spectral bandwidth of 50 nm, offering an axial resolution of 8 - 9 μm in air. At an A-line rate of 29 kHz and a sample arm power level of 600 μW, the SD-OCT system offered a peak sensitivity of 98 dB at zero delay that decreased to 82 dB at the maximum ranging depth of 2.4 mm in air. Figure 5 represents side-by-side comparison of OFDI and SD-OCT images near the fovea and optic disc. Figures A1 - A4 were obtained from a 36-year-old Asian male, and Figs. B1 - B2 were from a 41-year-old Caucasian male. Evidently, the OFDI images exhibit considerably deeper penetration into the choroid compared to the SD-OCT images, whereas the higher axial resolution in the SD-OCT images provides better contrast between retinal layers. The apparently superior penetration of the OFDI system to the SD-OCT system is attributed to the lower absorption and scattering in RPE at 1050 nm than 840 nm [15] as well as the higher sensitivity of OFDI at large depth. However, verifying this hypothesis would require detailed analysis involving more human subjects and imaging systems.

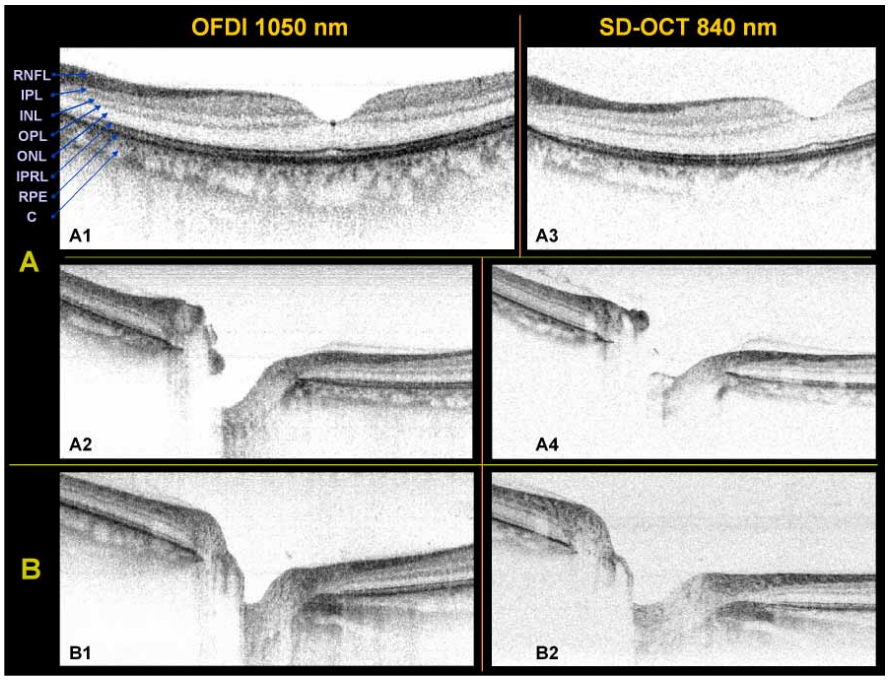

Fig. 5. Comparison of two imaging systems (OFDI at 1050 nm and SD-OCT at 840 nm). **A1** and **A2**: OFDI images at fovea and optic nerve head, respectively, from volunteer A, 36-year-old Asian male. **A3** and **A4**: SD-OCT images from the same volunteer at similar tissue locations. **B1** and **B2**: OFDI and SD-OCT images, respectively, obtained from volunteer B, 41-year-old Caucasian male. OFDI images exhibit considerably deeper penetration in tissue than SD-OCT images in all the data sets. The OFDI image (**A1**) shows the anatomical layered structure: RNFL; retinal nerve fiber layer, IPL; inner plexiform layer, INL; inner nuclear layer, OPL; outer plexiform layer, ONL; outer nuclear layer, IPRL; interface between the inner and outer segments of the photoreceptor layer, RPE; retinal pigmented epithelium, and C; choriocapillaris and choroid.

#68653 - $15.00 USD Received 7 March 2006; revised 25 April 2006; accepted 27 April 2006

3.4 Visualizing retinal and choroidal vasculature with OFDI

Given three-dimensional tomographic data of the eye's posterior segment, integrating the pixel values along the depth readily produces a two-dimensional fundus-type reflectivity image [28, 29]. Figure 6(a) depicts an integrated reflectivity image generated from the entire OFDI image sequence shown in Fig. 4. The image visualizes the optic nerve head, fovea, retinal vessels, and the faint outline of the deep choroidal vasculature; however, the depth information is completely lost. To overcome this limitation of the conventional method, we integrated only selective regions based on anatomical structures. For example, to visualize the retinal vasculature selectively with improved contrast, we used automatic image segmentation techniques [29] and integrated the reflectivity in the range between IPRL and RPE (marked by red lines in Fig. 6(b)), where the shadow or loss of signal created by the retinal vessels above appears most distinctly [28]. Integrating over the entire retina including the vessel often results in a lower contrast in the vasculature because retinal blood vessels produce large signals by strong scattering. Figure 6(c) depicts the resulting fundus-type image (shadow) of the retinal vessels. The choriocapillary layer contains abundant small blood vessels and pigment cells [30, 31]. Using a thin integration region in the upper part of choroid (labeled D in Fig. 6(b)), we also obtained an image of the choriocapillary layer (Fig. 6(d)). In contrast to retinal vessels, choroidal vessels appear as low-signal regions compared to their surroundings. The reason for this phenomenon has not been fully understood yet. To obtain an image

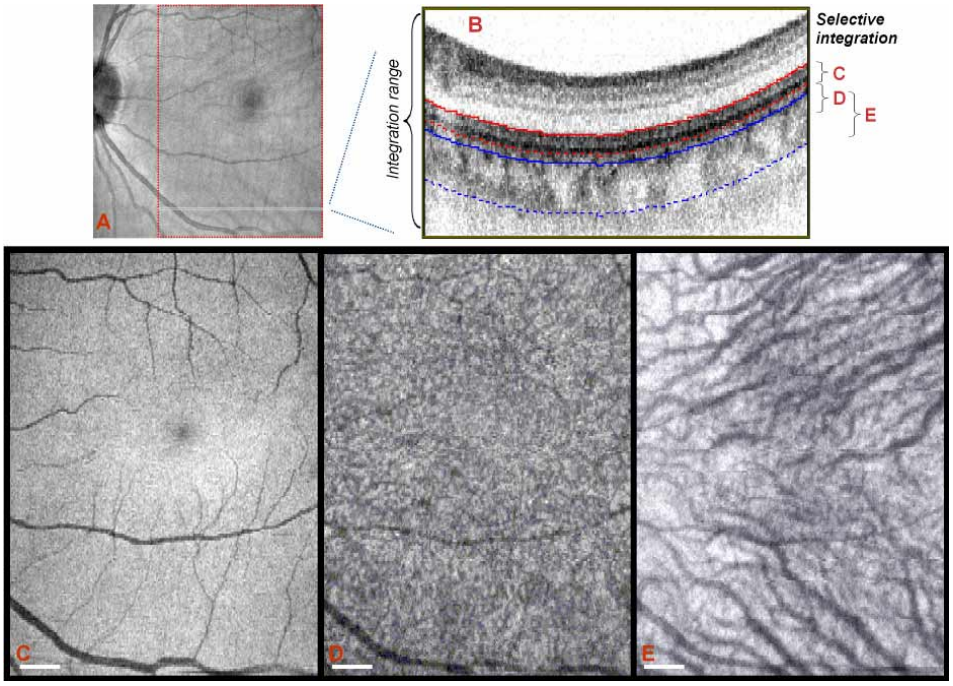

Fig. 6. The retinal and choroidal vasculature extracted from the three-dimensional OFDI data set (Fig. 4). (**A**) Two-dimensional reflectivity image (5.3 x 5.2 mm^2) obtained with the conventional full-range integration method. Higher (lower) reflectivity is represented by white (black) in the grayscale. (**B**) Illustration of the depth-sectioning integration method, with the different integration regions labeled C,D,E corresponding to the following fundus-type reflectivity images, respectively: (**C**) retinal reflectivity image showing the shadow of retinal vasculature (3.8 x 5.2 mm^2), (**D**) reflectivity image obtained from the upper part of the choroid, and (**E**) reflectivity image from the center of the choroid revealing the choroidal vasculature. Shadows of retinal vasculature are also visible in D and E. Scale bars: 0.5 mm.

#68653 - $15.00 USD Received 7 March 2006; revised 25 April 2006; accepted 27 April 2006

of the complete choroid region, we used the bottom integration region (marked by blue lines in Fig. 6(b)). The choroidal vasculature is clearly visualized in the resulting reflectivity image (Fig. 6(e)). Reflectivity images with similar qualities were obtained for volunteer B.

4. Discussion

Our experimental results convincingly show that OFDI at 1050 nm is a promising new technology that enables comprehensive imaging of human retina and choroid with high resolution and contrast. Our OFDI system offers an order-of-magnitude higher image acquisition speed than conventional time-domain OCT systems and provides deeper choroid penetration in comparison to a state-of-the-art spectral-domain OCT system at 840 nm. The improved penetration may be clinically useful for evaluating early stages of retinal pathologies such as age-related macular degeneration that are accompanied by choroidal neovascularization [15, 31]. Our system's enhanced penetration allowed us to obtain depth-sectioned fundus-type reflectivity images of the choroidal capillary and vascular networks. Fundus cameras [32] and scanning laser ophthalmoscopes [33] have traditionally been used to view vasculatures; however, these methods often require indocyanine green angiography [34] to get access to the choroid except for subjects with a low level of pigmentation.

The key enabling element of our OFDI system is the wavelength-swept laser we developed using a commercial SOA and a custom-built intracavity scanning filter. The laser's output power, tuning speed and range were sufficient to yield a high sensitivity of 98 dB, A-line rate of 18.8 kHz, and resolution of 10 μm in tissue. Increasing the saturation power and gain of SOA and reducing the extended-cavity loss can further improve the sensitivity (output power) and resolution (tuning range).

In conclusion, we have introduced a new OFDI technology that allows for comprehensive imaging of human retina, optic disc, and choroid *in vivo*, demonstrating its potential in clinical ophthalmic applications.

Acknowledgments

E.C.W. Lee is a Master of Science candidate in Electrical Engineering at the Massachusetts Institute of Technology (MIT) and acknowledges a scholarship from Natural Sciences and Engineering Council of Canada (NSERC). This work was supported in part by the National Institute of Health grant R33 CA110130, R01 EY14975, and R01 RR19768.

#68653 - $15.00 USD Received 7 March 2006; revised 25 April 2006; accepted 27 April 2006